Electronic Supplementary Information for

Constructing anion vacancies riched MoSSe/G van der Waals heterostructures for high-performance Mg-Li hybrid-ion batteries

Xianbo Yu,[a] Guangyu Zhao,[ab] Canlong Wu,[a] Huihuang Huang,[a] Chao Liu,[a] Xiaojie Shen,[a] Ming Wang,[a] Xiaoming Bai[a] and Naiqing Zhang*[ab]*

[a]State Key Laboratory of Urban Water Resource and Environment, School of Chemistry and Chemical Engineering, Harbin Institute of Technology, Harbin 150001, China

[b]Academy of Fundamental and Interdisciplinary Sciences, Harbin Institute of Technology, Harbin 150001, China.

E-mail: zhaogy810525@gmail.com; znqmww@163.com

Experimental Details

Preparation of v-MoSSe/G

242 mg of sodium molybdate dihydrate ($Na_2MoO_4 \cdot 2H_2O$, ≥99.5%) was completed dissolved in 30 mL of water to obtain the solution-A. 760 mg of dopamine hydrochloride (DOPA-HCl, $C_8H_{12}ClNO_2$, ≥99.8%) was dispersed in 30 mL of water to obtain the solution-B. The liquid from solution-A was added drop by drop to solution-B and the whole process needed to stir. After that, 684 mg of thiourea (C_2H_4NS, ≥99.0%) was dissolved in the above suspension solution and then transferred into a Teflon-lined autoclave (100 mL). The hydrothermal reaction was conducted at 200°C

for 30 h. After cooled down to room temperature, the solid products (MoS_2-PDOPA) were washed by the water and absolute ethanol, and then dried at 60°C in vacuum. Finally, 120 mg of MoS_2-PDOPA and 200 mg of selenium power (Se, ≥99.99%) were evenly mixed and annealed in a tube furnace at 900°C for 3 h under H_2/Ar flow to obtain v-MoSSe/G.

Preparation of MoS_2/G, v-$MoS_{1.5}Se_{0.5}$/G, and v-$MoS_{0.6}Se_{1.4}$/G

MoS_2/G was synthesized by directly thermal treatment of MoS_2-PDOPA under 900°C for 3 h in H_2/Ar flow. To survey the effect of different molar ratio of S:Se on electrochemical measurement of LMIBs, another two samples were synthesized under the same conditions as preparation of v-MoSSe/G. To synthesized the v-$MoS_{1.5}Se_{0.5}$/G, 120 mg of MoS_2-PDOPA and 90 mg of selenium power were evenly mixed and annealed in a tube furnace at 900°C for 3 h under H_2/Ar flow. Similarly, v-$MoS_{0.6}Se_{1.4}$/G was prepared by annealed the mixed 120 mg of MoS_2-PDOPA and enough selenium power (360 mg) at 900°C for 3 h under H_2/Ar flow.

Structure Characterizations

XRD was recorded on a PANalytical X'Pert PRO with Cu Kα radiation (λ = 1.5418 Å) at 40 kV and 40 mA. The morphology was observed by SEM (Hitachi SU8010, 15 kV) and TEM (Tecnai G2 F30, 300 kV). Surface area was measured by the Micromeritics ASAP 2020. XPS and Raman spectra analyses were performed by using a spectrometer with Al Kα radiation (Nepean, ON) and Renishaw INVIA.

Electrochemical Measurements

A standard CR2025-type coin cell was used to measure all the electrochemical

performance of the electrodes. A microporous membrane (Celgard 2400) and a polished Mg plate were selected as separator and anode. The word electrode with the loading mass of 1.0 mg cm^{-2} contains the active material (80wt%), polyvinylidene difluoride (10wt%), and acetylene black (10wt%). The current collector was carbon fiber paper and the electrolyte contained all-phenyl complex (APC) (contains 2.133 g of $AlCl_3$, 16 mL of phenyl magnesium chloride (MgPhCl), 1.696 g of LiCl, and 24 mL of anhydrous tetrahydrofuran (THF) for LMIBs. All the batteries were measured ranged from 0.2 V to 2.0 V versus Mg^{2+}/Mg. EIS was measured in a frequency between 0.1−100 kHz. GITT is measured by the Neware system, and all the batteries were performed for 5 min discharge and 20 min relaxing time at 30 mA g^{-1}. The *D* is calculated by Fick' second law:[1,2]

$$D = \frac{4}{\pi\tau}\left(\frac{m_B V_m}{M_B S}\right)^2\left(\frac{\Delta E_s}{\Delta E_t}\right)^2 \#(1)$$

where ΔE_s is steady-state potential change by the current pulse. ΔE_t represents the potential change during the constant current. τ, S, M_B, m_B, and V_M are relaxing time of the test, contact area of electrode/electrolyte, molar mass, the mass, and molar volume, respectively.

Computational Details

Vienna *ab-initio* simulation package (VASP) was used to investigate the migration energy barriers and adsorption energy of all the samples. The gradient corrected exchange correlation interaction of electrons was simulated by the Perdew-Burke-Ernzerhof (PBE) functional under the projector augmented wave (PAW) method.[3,4] The cut-off energy, convergence criterion, and energy convergence are 400 eV, 0.05 eV/Å,

and 10^{-4} eV, respectively. The Mg^{2+}/Li^{+} diffusion was using the climbing image nudged elastic band method (CI-NEB).[5] This work used the bilayer model with 5×2×1 supercell, sampled with 1×2×1 Monkhorst-Pack grid.[6] The adsorption energy (ΔE_{ad}) is calculated by the following equation: $\Delta E_{ad} = (E_{host+Li/Mg} - E_{host} - E_{Li/Mg})$, where $E_{host+Li/Mg}$, E_{host}, and $E_{Li/Mg}$ represent the energy of the Li/Mg atom intercalated the host materials, the host materials, and per Li or Mg atom, respectively.

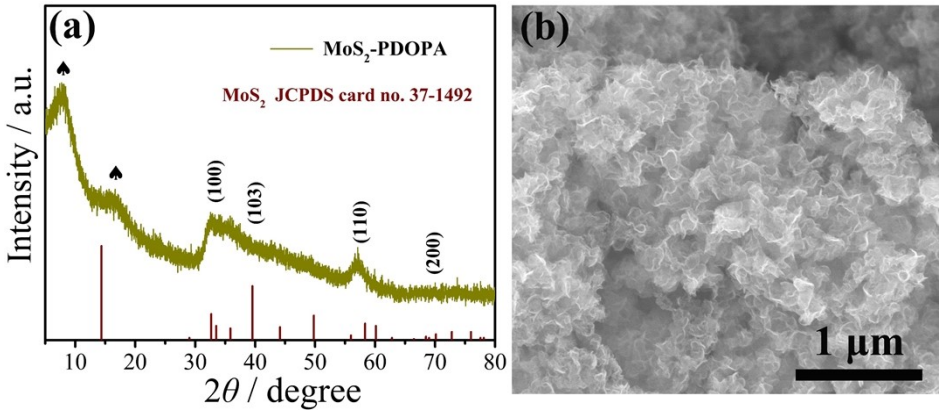

Fig. S1 (a) XRD pattern and (b) SEM image of MoS_2-PDOPA.

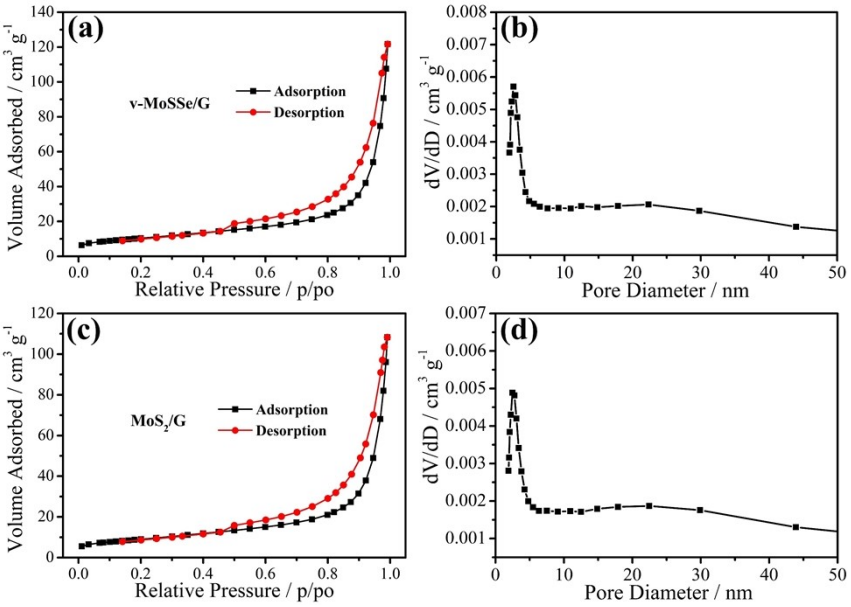

Fig. S2 (a,c) Nitrogen adsorption and desorption isotherms and (b,d) the corresponding pore-size distribution plots of v-MoSSe/G and MoS_2/G.

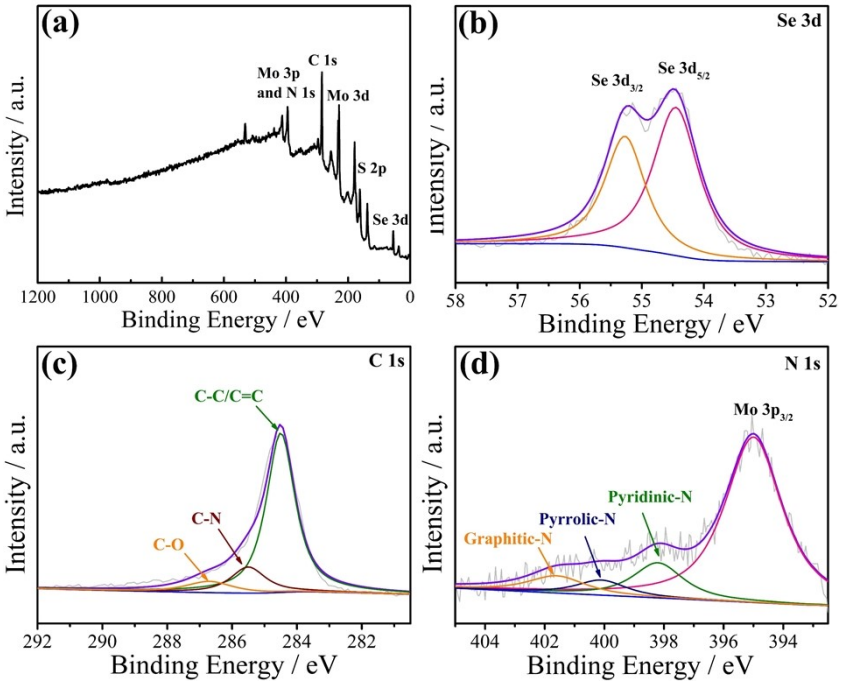

Fig. S3 XPS spectra of (a) survey, (b) Se 3d, (c) C 1s, and (d) N 1s of v-MoSSe/G.

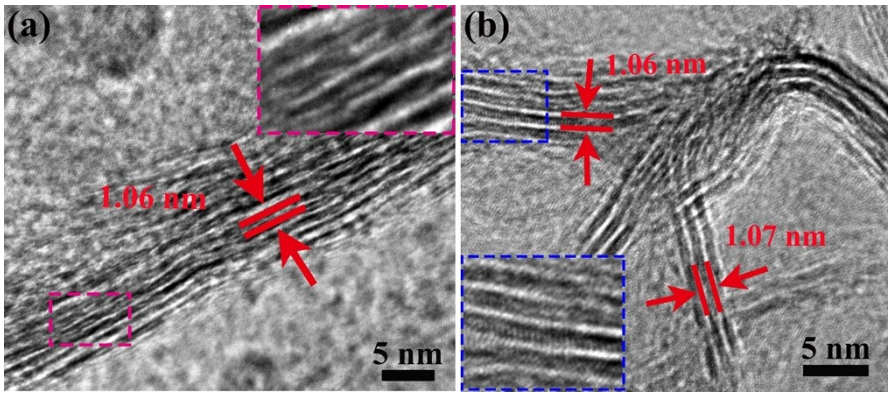

Fig. S4 HRTEM images of v-MoSSe/G.

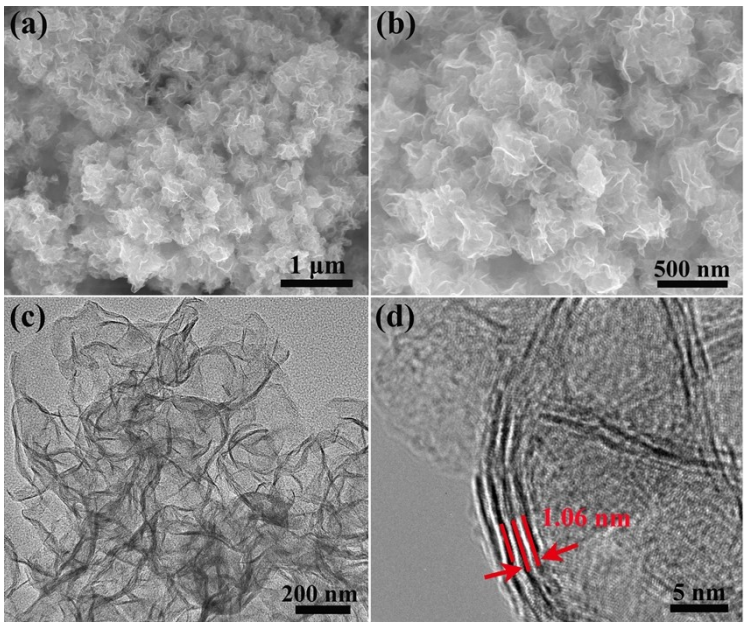

Fig. S5 (a,b) SEM, (c) TEM, and (d) HRTEM images of MoS_2/G.

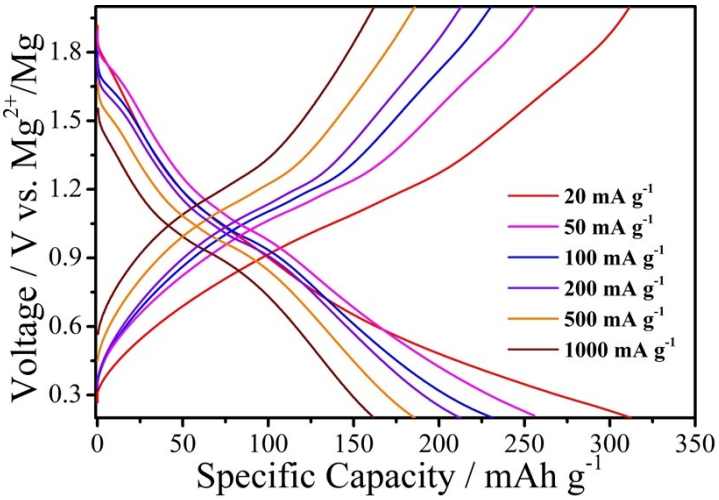

Fig. S6 Charge/discharge curves of v-MoSSe/G at different current densities.

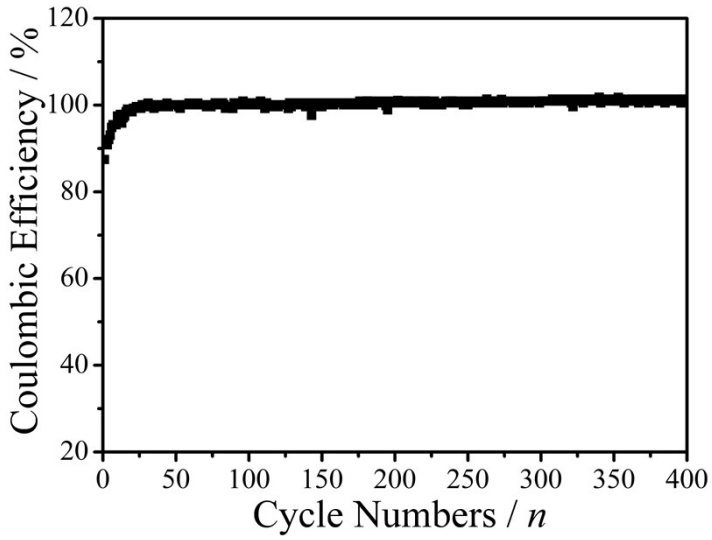

Fig. S7 Columbic efficiency of v-MoSSe/G for MIBs.

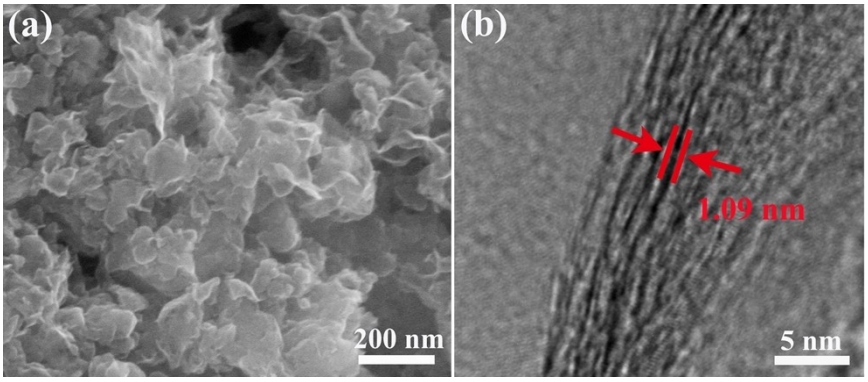

Fig. S8 (a) SEM and (b) HRTEM images of v-MoSSe/G after 200 cycles discharge.

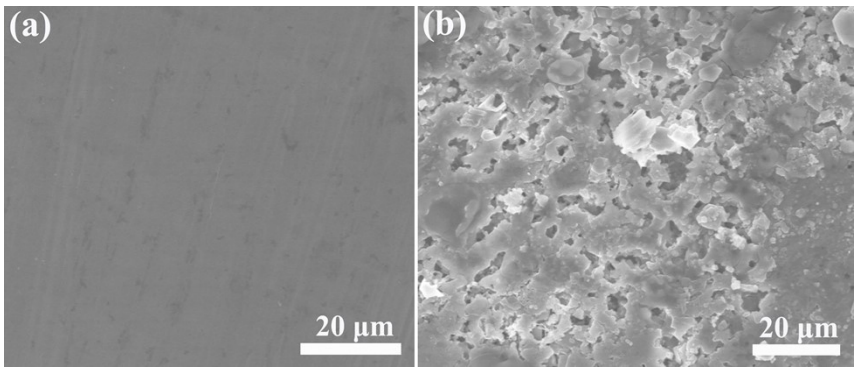

Fig. S9 SEM images for the surface of (a) pristine and (b) after 200 cycles of Mg anodes.

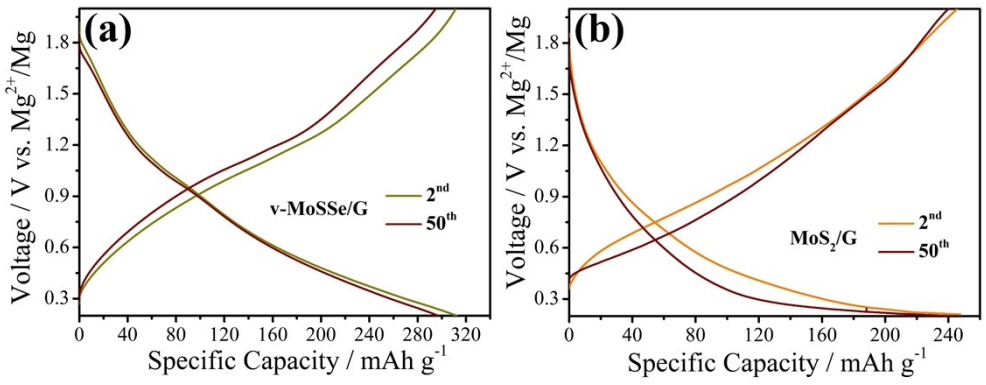

Fig. S10 Galvanostatic charge/discharge curves of (a) v-MoSSe/G and (b) MoS_2/G.

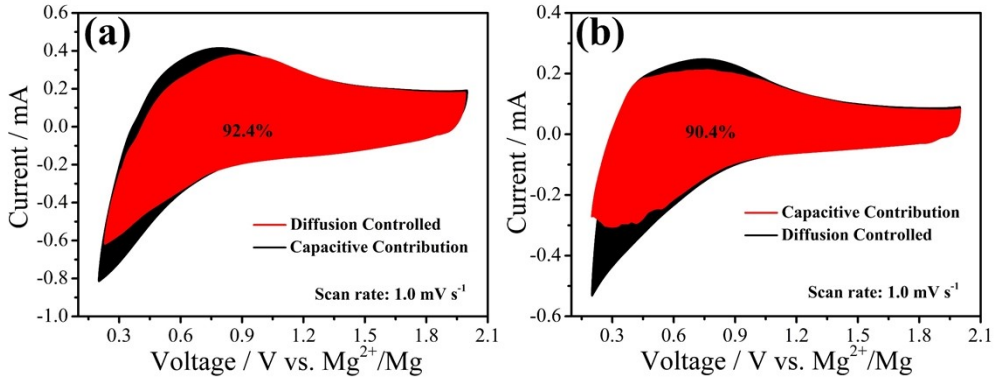

Fig. S11 The capacitive and diffusion-controlled contributions of (a) v-MoSSe/G and (b) MoS_2/G at the scan rate of 1.0 mV s^{-1}.

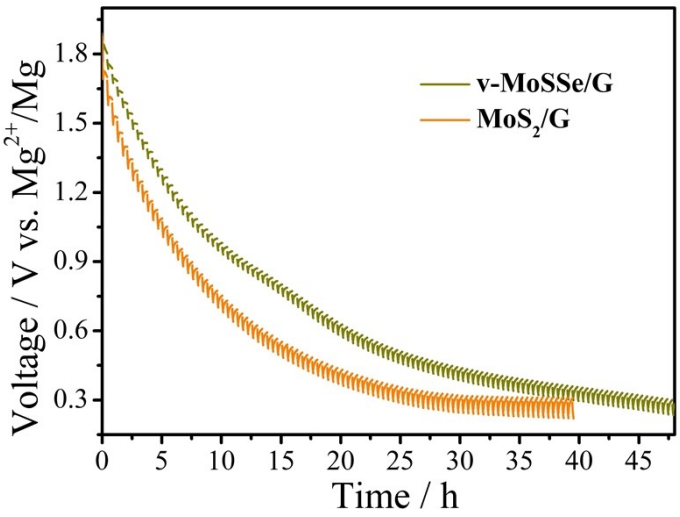

Fig. S12 GITT profiles of the discharge process of v-MoSSe/G and MoS_2/G.

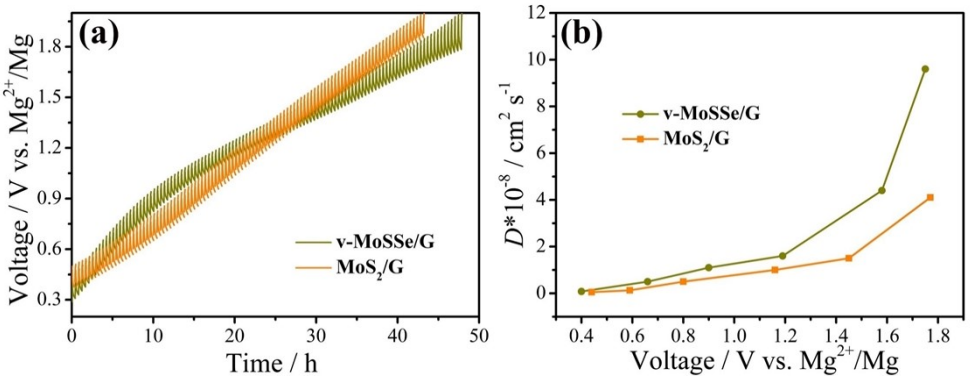

Fig. S13 (a) GITT profiles of the charge process and (b) the corresponding ion diffusion coefficient of v-MoSSe/G and MoS_2/G.

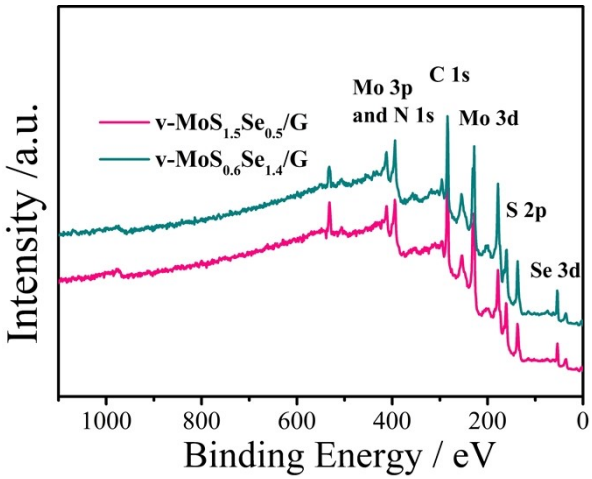

Fig. S14 Survey XPS spectra of v-$MoS_{1.5}Se_{0.5}$/G and (b) v-$MoS_{0.6}Se_{1.4}$/G.

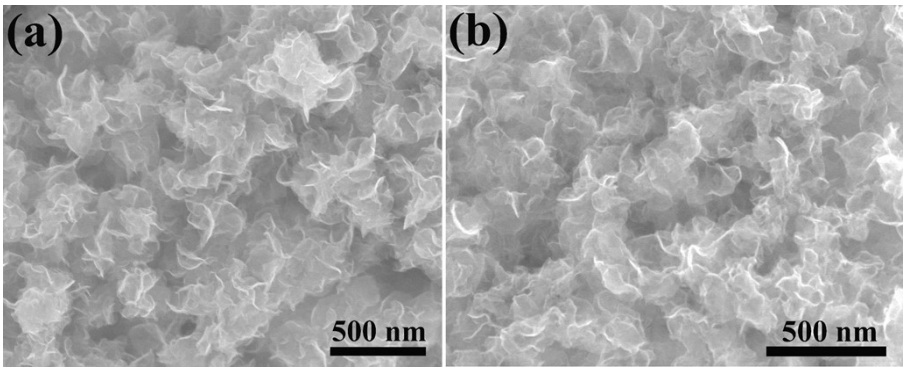

Fig. S15 SEM images of (a) v-$MoS_{1.5}Se_{0.5}$/G and (b) v-$MoS_{0.6}Se_{1.4}$/G.

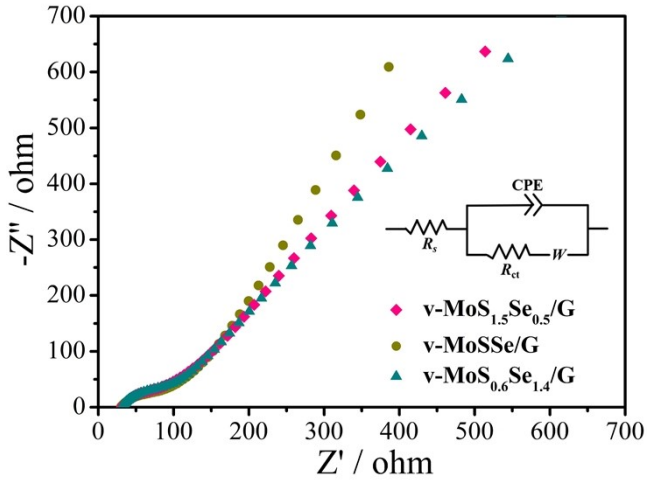

Fig. S16 Nyquist plots of v-MoSSe/G, v-$MoS_{0.6}Se_{1.4}$/G, and v-$MoS_{1.5}Se_{0.5}$/G after 20 cycles.

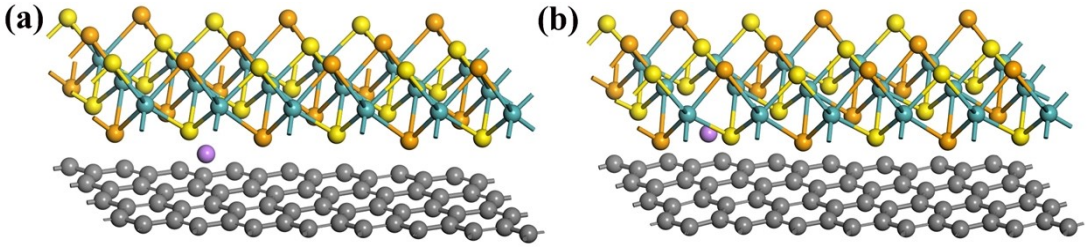

Fig. S17 Adsorption configurations of Li in (a) MoSSe/G and (b) 1Sev-MoSSe/G. Color code: Carbon (grey), sulfur (yellow), molybdenum (cyan), selenium (orange), and lithium (purple).

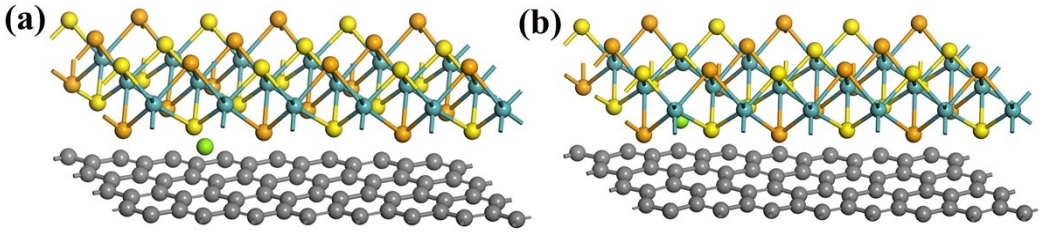

Fig. S18 Adsorption configurations of Mg in (a) MoSSe/G and (b) 1Sev-MoSSe/G. Color code: Carbon (grey), sulfur (yellow), molybdenum (cyan), selenium (orange), and Magnesium (green).

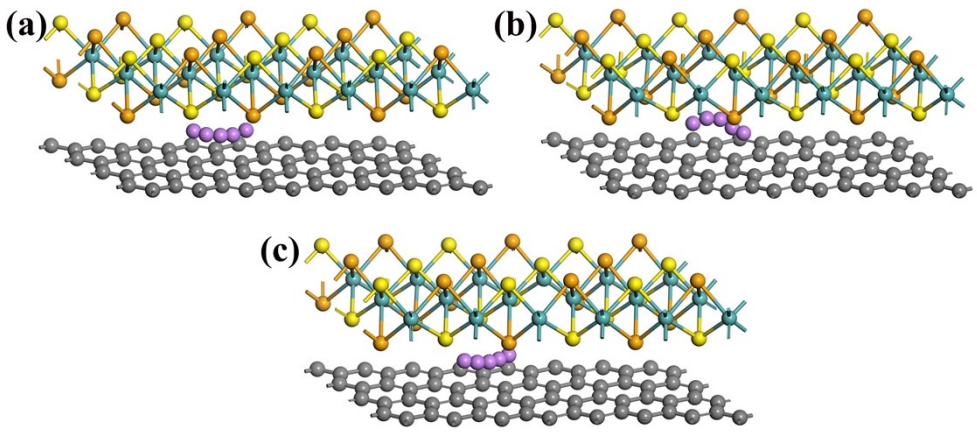

Fig. S19 Li diffusion paths in (a) MoSSe/G, (b) 1Sv-MoSSe/G, and (c) 1Sev-MoSSe/G. Color code: Carbon (grey), sulfur (yellow), molybdenum (cyan), selenium (orange), and lithium (purple).

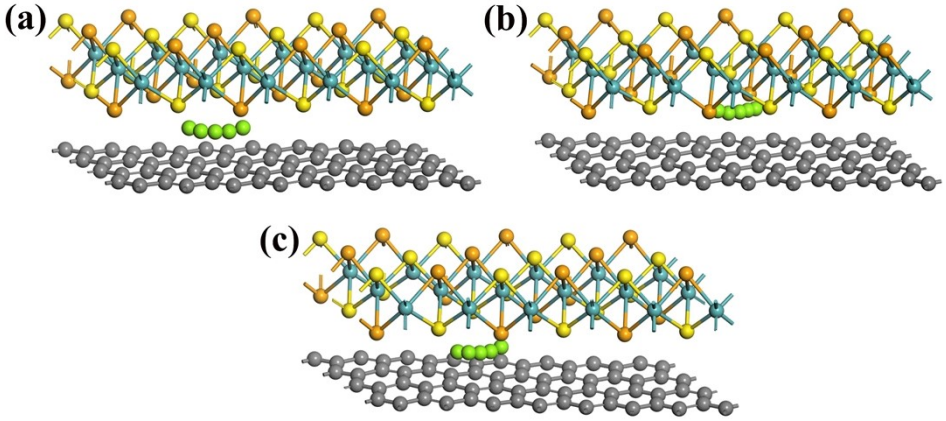

Fig. S20 Mg diffusion paths in (a) MoSSe/G, (b) 1Sv-MoSSe/G, and (c) 1Sev-MoSSe/G. Color code: Carbon (grey), sulfur (yellow), molybdenum (cyan), selenium (orange), and Magnesium (green).

Table S1. Comparison of electrochemical performance of v-MoSSe/G with other previously reported cathode materials for MLIBs.

Electrode material	Current Density (mA g^{-1})	Reversible Capacity (mAh g^{-1})	Cycle Numbers (*n*)	Whether Mg^{2+}/Li^{+} Co-intercalation	Ref.
MoS_2 Nano Flowers	1000	107	2300	No	[7]
MoS_2/G VH	20 1000	260.8 145.8	200 2200	Yes	[8]
$MoSe_2$/C	200	89	100	No	[9]
V_2MoO_8	20	135	50	Yes	[10]
TiS_2	80	160	400	No	[11]
$Li_3V_2(PO_4)_3$	100	135	200	No	[12]
$Li_4Ti_5O_{12}$	60	~125	500	Yes	[13]
VS_2-GO	90	200	100	No	[14]
VO_2	20	154.9	100	No	[15]
$LiCrTiO_4$	20	~125	30	No	[16]
V_2C MXene	50	~110	480	Yes	[17]
Cu_2Se **Cu_2Se/rGO**	26 26	~110 ~65	30 100	No	[18]
$Ti_3C_2T_x$/CNT	100	~80	500	No	[19]
MoS_2/G	20 1000	220.9 126.9	400 3000	Yes	This work
v-MoSSe/G	**20** **1000**	**299.2** **164.6**	**400** **3000**	**Yes**	**This work**

References

[1] M. Ma, S. Zhang, Y. Yao, H. Wang, H. Huang, R. Xu, J. Wang, X. Zhou, W. Yang,

Z. Peng, X. Wu, Y. Hou, Y. Yu, Heterostructures of 2D molybdenum dichalcogenide on 2D nitrogen-doped carbon: superior potassium-ion storage and insight into potassium storage mechanism, Adv. Mater. 32 (2020) 2000958.

[2] N. Liu, X. Wu, L. Fan, S. Gong, Z. Guo, A. Chen, C. Zhao, Y. Mao, N. Zhang, K. Sun, Intercalation Pseudocapacitive Zn^{2+} Storage with Hydrated Vanadium Dioxide toward Ultrahigh Rate Performance. *Adv. Mater.* 32 (2020) 1908420.

[3] P. E. Blöchl, Projector augmented-wave method, Phys. Rev. B 50 (1994) 17953−17979.

[4] G. Kresse, D. Joubert, From ultrasoft pseudopotentials to the projector augmented-wave method, Phys. Rev. B 59 (1999) 1758−1775.

[5] G. Henkelman, B.P. Uberuaga, H. Jónsson, A climbing image nudged elastic band method for finding saddle points and minimum energy paths, J. Chem. Phys. 113 (2000) 9901−9904.

[6] H.J. Monkhorst, J.D. Pack, Special points for brillouin-zone integrations, Phys. Rev. B 13 (1976) 5188−5192.

[7] Y. Ju, Y. Meng, Y. Wei, X. Bian, Q. Pang, Y. Gao, F. Du, B. Liu, G. Chen, Li^{+}/Mg^{2+} hybrid-ion batteries with long cycle life and high rate capability employing MoS_2 nano flowers as the cathode material, Chem. Eur. J. 22 (2016) 18073−18079.

[8] X. Yu, G. Zhao, C. Liu, C. Wu, H. Huang, J. He, N. Zhang, A MoS_2 and graphene alternately stacking van der Waals heterostructure for Li^{+}/Mg^{2+} co-intercalation, Adv. Funct. Mater. 31 (2021) 2103214.

[9] J.-J. Fan, S.-Y. Shen, Y. Chen, L.-N. Wu, J. Peng, X.-X. Peng, C.-G. Shi, L.

Huang, W.-F. Lin, S.-G. Sun, A rechargeable Mg^{2+}/Li^{+} hybrid battery based on sheet-like $MoSe_2$/C nanocomposites cathode, Electrochem. Commun. 90 (2018) 16−20.

[10] X. Miao, Z. Chen, N. Wang, Y. Nuli, J. Wang, J. Yang, S. Hirano, Electrospun V_2MoO_8 as a cathode material for rechargeable batteries with Mg metal anode, Nano Energy 34 (2017) 26−35.

[11] T. Gao, F. Han, Y. Zhu, L. Suo, C. Luo, K. Xu, C. Wang, Hybrid Mg^{2+}/Li^{+} battery with long cycle life and high rate capability, Adv. Energy Mater. 5 (2015) 1401507.

[12] M. Rashad, H. Zhang, X. Li, H. Zhang, Fast kinetics of Mg^{2+}/Li^{+} hybrid ions in a polyanion $Li_3V_2(PO_4)_3$ cathode in a wide temperature range, J. Mater. Chem. A 7 (2019) 9968−9976.

[13] N. Wu, Z.-Z. Yang, H.-R. Yao, Y.-X. Yin, L. Gu, Y.-G. Guo, Improving the electrochemical performance of the $Li_4Ti_5O_{12}$ electrode in a rechargeable magnesium battery by lithium-magnesium co-intercalation, Angew. Chem. Int. Ed. 54 (2015) 5757−5761.

[14] R. Sun, C. Pei, J. Sheng, D. Wang, L. Wu, S. Liu, Q. An, L. Mai, High-rate and long-life VS_2 cathodes for hybrid magnesium-based battery, Energy Storage Mater. 12 (2018) 61–68.

[15] C. Pei, F. Xiong, J. Sheng, Y. Yin, S. Tan, D. Wang, C. Han, Q. An, L. Mai, VO_2 nanoflakes as the cathode material of hybrid magnesium-lithium-ion batteries with high energy density, ACS Appl. Mater. Interfaces 9 (2017) 17060−17066.

[16] Y. Yao, L. Zhang, X. Bie, H. Chen, C. Wang, F. Du, G. Chen, Exploration of spinel $LiCrTiO_4$ as cathode material for rechargeable Mg-Li hybrid batteries, Chem. Eur. J. 23 (2017) 17935−17939.

[17] F. Liu, Y. Liu, X. Zhao, K. Liu, H. Yin, L.-Z. Fan, Prelithiated V_2C MXene: A high-performance electrode for hybrid magnesium/lithium-ion batteries by ion cointercalation. Small 16 (2020) 1906076.

[18] H. Yuan, N. Wang, Y. NuLi, J. Yang, J. Wang, Hybrid Mg^{2+}/Li^{+} batteries with Cu_2Se cathode based on displacement reaction, Electrochim. Acta 261 (2018) 503−512.

[19] A. Byeon, M.-Q. Zhao, C.E. Ren, J. Halim, S. Kota, P. Urbankowski, B. Anasori, M.W. Barsoum, Y. Gogotsi, Two-dimensional titanium carbide MXene as a cathode material for hybrid magnesium/lithium-ion batteries, ACS Appl. Mater. Interfaces 9 (2017) 4296−4300.